

**Quasi-two-dimensional dipolar fluid at low densities: Monte Carlo simulations and theory**J. M. Tavares,<sup>1,2</sup> J. J. Weis,<sup>3</sup> and M. M. Telo da Gama<sup>1</sup><sup>1</sup>*Centro de Física da Matéria Condensada da Universidade de Lisboa, Avenida Professor Gama Pinto 2, P-1649-003 Lisbon, Portugal*<sup>2</sup>*Universidade Aberta, Rua Fernão Lopes, 9, 2º D, P-1000-132 Lisbon, Portugal*<sup>3</sup>*Laboratoire de Physique Théorique, Université de Paris XI, Bâtiment 210, F-91405, Orsay Cedex, France*

(Received 26 February 2002; published 20 June 2002)

We studied a quasi-two-dimensional dipolar fluid in the chaining regime using Monte Carlo canonical simulations and theoretical analyses. The self-assembled clusters were characterized by measuring their internal energy, conformational properties, and equilibrium length distributions. We generalized and used equilibrium polymer theory to describe the structure of the chains and rings observed in the simulations. The scaling forms of the length distribution functions predicted by theory were found to describe adequately the simulation results. Finally, we discuss how this type of analysis may be used to establish the existence and mechanisms of phase transitions in dilute dipolar fluids.

DOI: 10.1103/PhysRevE.65.061201

PACS number(s): 61.20.Ja, 61.20.Gy, 75.50.Mm, 68.65.-k

**I. INTRODUCTION**

Interest in the dipolar hard sphere fluid has grown in the last decade owing to its unusual chained structure, to the absence of a standard liquid-vapor transition, and to the relation between the structural and thermodynamic properties of this system.

The self-assembly of chains, observed in Monte Carlo simulations of the dipolar fluid at low temperatures and densities (e.g., [1–5]), is driven by short-ranged anisotropic correlations that constitute a challenge to the standard theories used in calculations of the thermodynamics of simple fluids. In fact, the thermodynamic properties of the dipolar fluid under these conditions cannot be calculated using simple mean field approximations. On the other hand, integral equation theories capture some features of the pair correlation function but are not reliable as far as calculations of the thermodynamic properties are concerned. By contrast, association theories have been applied successfully to this problem since, by construction, they include the contribution of the chained structure to the thermodynamics. These theories consider the dipolar fluid as a mixture of polydisperse chains and write the free energy as a functional of the set of chain densities. The equilibrium chain length distribution function is obtained by minimizing the free energy functional, at fixed temperature and (monomer) density, with respect to the chain densities [6–9]. This approach has proved very useful in describing several aspects of the simulation results, namely, the slow variation of the internal energy with density [7], the absence of a liquid-vapor phase transition [3,6,8,10,11], and the dependence of the critical density on the ratio of isotropic to dipolar interactions in models that include attractive isotropic interactions [3,8,12].

Recently, a direct calculation of the free energy using canonical Monte Carlo (MC) simulations, at several temperatures, suggested the existence of one (or two) isotropic fluid-fluid transitions at low densities [13]. The existence of at least one phase transition was corroborated by isobaric and grand canonical MC simulations at a single temperature [13]. These results led Tlustý and Safran [14] to propose a new mechanism for the phase transition of dipolar fluids at low

densities and temperatures: the competition between a (low density) phase rich in chains and entropically favorable, and a (higher density) phase rich in defects (the junction of three chain ends and thus called Y defects [15]) and energetically favorable. From the structural point of view, this transition differs from the standard liquid-vapor transition and resembles the structural or topological phase transition proposed by the same authors to describe the emulsification failure observed in microemulsions [16]. A comparison of the structure observed in simulations of dipolar fluids with that responsible for the mechanism proposed in [14] has not been carried out and thus the existence and mechanisms of the phase transition in dilute dipolar fluids remain open problems. In fact, in simulations where the chain structure was analyzed [1] defects (branching of chains) were rarely observed [17].

The simulations and theoretical work referred to above were carried out for the dipolar fluid in three dimensions (3D). In this paper we report simulation and theoretical results for a quasi-two-dimensional (2D) hard sphere dipolar fluid: a 3D dipolar fluid with the centers of mass and dipole moments constrained to a plane [18]. We chose to consider this model since in 2D defect formation is clearly observed. In addition, ring formation (not present or only marginally present in 3D) also occurs in 2D and thus we develop and test a generalization of the theoretical analyses used previously [4,6,8,14]. Finally, the reduced dimensionality allows longer simulations of larger systems which are required to obtain accurate equilibrium distributions for the various types of self-assembled clusters (chains, rings, and defect clusters). In a different context, this model is useful in connection with recent experiments [19] that reported the observation of rings, chains, and defects in monolayers of spherical monodispersed colloidal magnetic particles.

In this paper, we aim to describe accurately the structure of the quasi-2D dipolar fluid at low densities, namely, the ring and chain length equilibrium distributions observed in computer simulations. This will be done by using equilibrium polymer theory (e.g., [20,21]) and can be viewed as a generalization of the association theories used in earlier work [4,6,8]. We will discuss the extent to which these results may

be used to clarify the existence of phase transitions in dilute dipolar fluids and to establish the mechanisms driving them.

The paper is organized as follows. In Sec. II, we describe the model, the details of the canonical Monte Carlo simulations and the algorithms employed to identify the clusters. The characterization of the clusters is carried out in Sec. III, where we report results for their internal energy, conformational properties, and the equilibrium length distributions of chains and rings. In Sec. IV, we describe briefly equilibrium polymer theory and use it to describe the structure of dipolar chains and rings observed in the simulations. We compare the scaling predicted theoretically with that observed in the simulated length distribution functions of chains and rings. Finally, in Sec. V, we conclude by discussing how our analysis may be used to establish the existence of a phase transition in this system.

## II. MODEL AND MONTE CARLO SIMULATIONS

The dipolar hard sphere model is a system of hard spheres of diameter  $\sigma$  with an embedded point dipole of strength  $\mu$  interacting through the pair potential

$$\phi_{DHS} = \begin{cases} \infty, & r_{12} < \sigma, \\ -\frac{\mu^2}{r_{12}^3} [3(\hat{\mu}_1 \cdot \hat{r}_{12})(\hat{\mu}_2 \cdot \hat{r}_{12}) - \hat{\mu}_1 \cdot \hat{\mu}_2], & r_{12} \geq \sigma. \end{cases} \quad (1)$$

$r_{12}$  is the distance between the centers of the spheres 1 and 2,  $\hat{r}_{12} \equiv (\vec{r}_2 - \vec{r}_1)/r_{12}$  the unit interparticle vector, and  $\hat{\mu}_1, \hat{\mu}_2$  the unit vectors in the direction of the dipole moments of spheres 1 and 2, respectively. In the simulations reported in this paper, the centers of the spheres and their dipole moments are constrained to lie on the same plane, and thus the model is a quasi-2D dipolar hard sphere fluid. We define the reduced density as  $\rho^* \equiv \sigma^2 N/A$ , where  $N$  is the number of spheres in the system with area  $A$ , and the reduced dipole moment (or square root of the inverse reduced temperature) as  $\mu^* \equiv \mu/\sqrt{\sigma^3 k_B T}$ , where  $k_B$  is Boltzmann's constant and  $T$  the absolute temperature.

The MC simulations were performed in the canonical ( $N$ - $V$ - $T$ ) ensemble using 1600 and in most cases 5776 particles, in a square box with periodic boundary conditions. An Ewald sum was used to account for the long range of the dipole-dipole interaction; for a 3D dipolar interaction with the centers of the spheres constrained to a 2D lattice, the sum is absolutely convergent and is given by [22,23]

$$U = -\frac{1}{2} \sum_{i=1}^N \sum_{j=1}^N \sum_{\mathbf{n}}' [B(|\mathbf{r}_{ij} + \mathbf{n}|) \boldsymbol{\mu}_i \cdot \boldsymbol{\mu}_j + C(|\mathbf{r}_{ij} + \mathbf{n}|) \times (\boldsymbol{\mu}_i \cdot \mathbf{r}_{ij})(\boldsymbol{\mu}_j \cdot \mathbf{r}_{ij})] + \frac{\pi}{A} \sum_{\mathbf{G} \neq \mathbf{0}} \frac{\text{erfc}(G/2\alpha)}{G} F(\mathbf{G}) F^*(\mathbf{G}) - \frac{2\alpha^3}{3\sqrt{\pi}} \sum_{i=1}^N (\mu_i)^2, \quad (2)$$

where the functions  $B(r)$  and  $C(r)$  are

$$B(r) = -\frac{\text{erfc}(\alpha r)}{r^3} - \frac{2\alpha}{\sqrt{\pi}} \frac{\exp(-\alpha^2 r^2)}{r^2}, \quad (3)$$

$$C(r) = 3 \frac{\text{erfc}(\alpha r)}{r^5} + \frac{2\alpha}{\sqrt{\pi}} \left( \frac{3}{r^2} + 2\alpha^2 \right) \frac{\exp(-\alpha^2 r^2)}{r^2}, \quad (4)$$

while

$$F(\mathbf{G}) = \sum_{i=1}^N (\mathbf{G} \cdot \boldsymbol{\mu}_i) \exp[i\mathbf{G} \cdot \mathbf{r}_i]. \quad (5)$$

In Eq. (2)  $\vec{r}_{ij} = \vec{r}_j - \vec{r}_i$ ,  $L = \sqrt{A}$  is the box length, and  $\text{erfc}$  denotes the complementary error function. The prime in the sum over  $\mathbf{n} = (n_x, n_y)$ , with  $n_x, n_y$  integers, restricts it to  $i \neq j$  for  $\mathbf{n} = \mathbf{0}$ . With  $\alpha = 6.5/L$ , adopted in our calculations, only terms with  $\mathbf{n} = \mathbf{0}$  need to be retained in Eq. (2). The sum in reciprocal space extends over all lattice vectors  $\mathbf{G} = 2\pi\mathbf{n}/L$  with  $|\mathbf{n}|^2 \leq n_{max}^2 = 64$  while the sum in real space is truncated at about  $13\sigma$ .

As will be apparent below, in the range of dipole moments  $2.5 \leq \mu^* \leq 3$  the dipolar spheres self-assemble into strongly bonded structures (clusters) consisting of linear chains, rings, and more complicated structures where different chains and/or rings are connected (we shall call these defect clusters irrespective of their precise topology). Sampling of phase space was achieved by performing both single-particle and cluster moves. The latter considerably enhance convergence by bringing clusters more rapidly into contact, thereby creating defects (contact of more than two particles), which were found to be the major mechanism for breaking and rearranging clusters.

Single-particle trial moves were performed in cycles, each cycle corresponding to the displacement of all  $N$  particles and the rotation of their dipole moments with amplitudes adjusted to give an acceptance ratio of about 0.3. Every 6000 cycles for the 5776 particle system or 20 000 cycles for the smaller system, a cluster move was carried out by displacing the centers of mass of all clusters uniformly in a square with side  $(10-12)\sigma$ . In order to satisfy detailed balance cluster moves resulting in a cluster larger than the displaced one were rejected. We use an operational definition of the clusters: a particle belongs to a given cluster if its nearest-neighbor distance within that cluster is less than a cutoff distance  $r_c$ . Note that at this stage there is no need to distinguish between different cluster topologies. Calculations were started from an initial configuration with monomers only. Equilibration was assumed to obtain when the variation of the total energy of the system was less than 2–3%. Owing to the very slow rate of convergence this led us to discard typically of the order of  $(4-5) \times 10^6$  cycles for the 5776 system. After equilibration, of the order of 50–100 configurations separated by 150 000–200 000 cycles for the 5776-particle system and of the order of 100–200 configurations separated by 300 000–1 000 000 cycles for the 1600-particle system were kept for later analysis of the structural properties of the clusters. For most thermodynamic states averages were taken

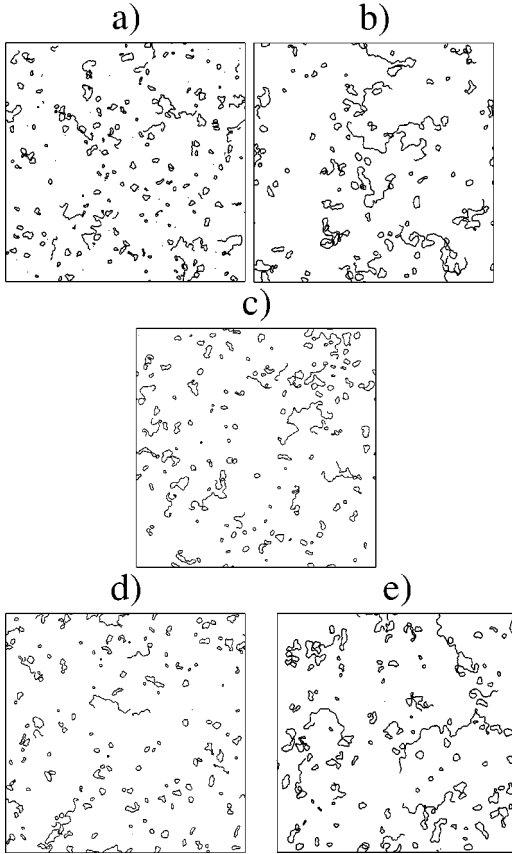


FIG. 1. Snapshots of equilibrium configurations obtained from canonical Monte Carlo simulations of the quasi-2D dipolar fluid. For (a), (b), and (c) the reduced density is  $\rho^*=0.03125$  and the reduced dipole moments are  $\mu^*=2.5, 3,$  and  $2.75$ , respectively. For (d) and (e) the dipole moment is  $\mu^*=2.75$  and the densities are  $\rho^*=0.025$  and  $0.0375$ , respectively.

over three independent runs, consisting of heating a configuration to a state with monomers only and then cooling it down to the desired temperature.

In order to check the time evolution of the clusters within a simulation run we recorded the lifetime of pairs of bonded particles. At  $\mu^*=2.5$ , 50% of the bonds are broken (and reassembled) in  $1 \times 10^6$  cycles while almost 90% of them do not survive  $5 \times 10^6$  cycles. At dipole moment 2.75, however, the lifetime of bonds increases by almost an order of magnitude. As a result, for the simulation with 5776 particles only 65% of the bonds were broken and reassembled during the rather long simulation run. These numbers are almost independent of density. The bond lifetimes increase dramatically if cluster moves are not used.

In Fig. 1 we plot snapshots of characteristic equilibrium configurations for different densities and dipole moments. They clearly show that, for these thermodynamic states, the dipolar spheres self-assemble to form aggregates of different sizes. A more careful look distinguishes various types of aggregates. Some exhibit linear aggregation only (every particle is bonded at most to two other particles) and are closed (rings) or open (chains). All the other aggregates are more complex and exhibit branching, even if most of their particles are still linearly aggregated. These branching points are

called defects and the structures they belong to defect clusters. The defects exhibit a different number of branches (mostly 3 or 4, called Y and X defects, respectively, following [14]) and the corresponding clusters exhibit different topologies, depending on the number of “holes,” “ends,” and the type of defects. The snapshots of Fig. 1 may be used to infer the evolution of the dipolar fluid structure with increasing dipole moment at fixed density [sequence (a),(c),(b)]: the size of all clusters increases, chains almost disappear, the number of rings decreases, and at the lowest temperature the structure consists of very few large defect clusters with rather complex topology. The evolution of the structure with increasing density at a fixed dipole moment exhibits the same qualitative features, as seen in the sequence of snapshots (d),(c), and (e) of Fig. 1. Chaining or linear aggregation is to be expected due to the anisotropy of the dipolar interaction (see [9]). Defect formation was observed in 2D experiments [19], and was proposed on general grounds for 2D and 3D dipolar systems [14]. Simulations of 3D dipolar fluids, however, suggest little if any defect formation within the chaining regime.

A qualitative analysis of the “dynamics” of the equilibrium dipolar fluid was carried out by inspection of sequences of equilibrium snapshots. This revealed the existence of frequent events that drive the equilibrium “dynamics:” chain ends join to form a ring; a chain bends and attaches one of its ends to an interior particle, thereby forming a ring and a chain that subsequently detaches; two rings fuse into a larger ring; two chains come into contact and exchange branches; a ring is absorbed into a chain; two rings form from a larger ring; etc. This analysis also showed that small rings and chains are very stable and do not break spontaneously.

The qualitative picture of the structure in terms of clusters may be quantified by generalizing a method used in [1,4]. The classification of clusters is carried out by calculating the first, second, and third nearest-neighbor distances (respectively,  $r_{1j}, r_{2j},$  and  $r_{3j}$ ) of each particle  $j$ : if  $r_{1j} > r_c$ ,  $j$  is a free particle; if  $r_{1j} < r_c$  and  $r_{2j} > r_c$ ,  $j$  is an end particle; if  $r_{2j} < r_c$  and  $r_{3j} > r_c$ , then  $j$  is an interior particle; and, finally, if  $r_{3j} < r_c$ ,  $j$  is a defect particle. A ring is a cluster with interior particles only, a chain a cluster with two (and only two) ends, and a defect cluster a cluster with at least one defect particle. For strongly bonded clusters (as occurs in the present system) a range of cutoff distances yields qualitatively similar results. Throughout this work we used  $r_c = 1.15\sigma$ . We will show later that our results are independent of this particular choice.

### III. RESULTS FROM MC SIMULATIONS: LENGTH DISTRIBUTIONS, INTERNAL ENERGY, AND CONFORMATIONAL PROPERTIES

#### A. General results

In Table I we summarize our results for the total energy and for some of the quantities characterizing the clusters. These results were obtained from simulations with  $N = 1600$  and  $N = 5776$  particles at reduced densities  $\rho^* = 0.025, 0.03125,$  and  $0.0375$  and reduced dipole moments  $\mu^* = 2.5, 2.75,$  and  $3.0$ .

TABLE I. Structure and energy of the quasi-2D dipolar fluid obtained from simulations.  $N$  is the total number of particles;  $U^*$  is the total reduced energy per particle,  $U^* = \beta U/N$ .  $\bar{N}_x$  is the mean length of the distribution for clusters of type  $x$ ,  $\phi_x$  is the fraction of particles in clusters of type  $x$ , and  $E_x^*$  is the reduced internal energy per particle in those clusters.  $c$ ,  $r$ , and  $cd$  refer to chains, rings, and defect clusters, respectively.  $U_{cl}^*$  is the average reduced internal energy per particle in clusters.

$\mu^*$	$\rho^*$	$N$	cycles/ $10^6$	$U^*/\mu^{*2}$	$U_{cl}^*/\mu^{*2}$	$\bar{N}_c$	$\phi_c$	$E_c^*/\mu^{*2}$	$\bar{N}_r$	$\phi_r$	$E_r^*/\mu^{*2}$	$\bar{N}_{cd}$	$\phi_{cd}$	$E_{cd}^*/\mu^{*2}$
2.5	0.025	1600	78	-1.992	-1.981	21	0.44	-1.941	22	0.39	-2.023	41	0.17	-1.990
2.5	0.025	5776	18	-1.986	-1.976	21	0.47	-1.938	22	0.33	-2.023	46	0.19	-1.987
2.5	0.03125	1600	50	-1.992	-1.986	23	0.46	-1.949	24	0.34	-2.029	47	0.20	-1.997
2.5	0.03125	5776	11	-1.988	-1.972	22	0.50	-1.938	21	0.27	-2.022	50	0.22	-1.988
2.5	0.0375	1600	84	-2.000	-1.985	24	0.47	-1.952	24	0.30	-2.028	53	0.23	-1.997
2.5	0.0375	5776	14	-1.993	-1.977	24	0.50	-1.946	22	0.26	-2.025	54	0.24	-1.991
2.75	0.025	1600	100	-2.097	-2.095	39	0.19	-2.070	32	0.63	-2.100	78	0.18	-2.101
2.75	0.025	5776	20	-2.092	-2.081	38	0.29	-2.051	27	0.45	-2.095	91	0.26	-2.089
2.75	0.03125	5776	13	-2.091	-2.082	42	0.29	-2.058	28	0.42	-2.096	91	0.29	-2.087
2.75	0.0375	1600	220	-2.097	-2.093	46	0.24	-2.072	34	0.50	-2.102	104	0.26	-2.097
2.75	0.0375	5776	13	-2.089	-2.082	44	0.29	-2.058	28	0.34	-2.097	109	0.37	-2.088
3.0	0.025	5776	28	-2.151	-2.149	55	0.09	-2.125	34	0.53	-2.151	117	0.38	-2.153
3.0	0.03125	5776	8	-2.150	-2.147	68	0.12	-2.125	33	0.33	-2.150	174	0.55	-2.149
3.0	0.0375	5776	36	-2.152	-2.151	67	0.09	-2.130	38	0.38	-2.153	180	0.53	-2.153

The reduced total internal energy per particle, divided by  $\mu^{*2}$ , decreases slightly with increasing dipole moment and is essentially independent of density, indicating that intercluster interactions are negligible. This is corroborated by a direct calculation of the average internal energy per particle in clusters ( $U_{cl}^*$  in Table I), which was found to be nearly the same as the total internal energy per particle. We have also calculated the internal energy per particle for each type of cluster. A comparison of these quantities shows that the internal energy of chains is the highest and that of rings the lowest. Defect clusters have an intermediate internal energy per particle that approaches that of chains and rings, for large clusters. Note that for a given thermodynamic state, the energy of the longer runs is always slightly lower. These differences, of the order of 1%, are systematic and result from the fact that the internal energy has not fully converged after the very large number of cycles of our simulation runs.

The mean chain length ( $\bar{N}_c$ ) increases while the fraction of particles in chains ( $\phi_c$ ) decreases with increasing dipole moment. Variations of these quantities with density are hard to detect but  $\bar{N}_c$  appears to increase with increasing density. The mean ring length ( $\bar{N}_r$ ) also increases with increasing dipole moment but more slowly than  $\bar{N}_c$ . The fraction of particles in rings  $\phi_r$  decreases with increasing density and its dependence on the dipole moment appears to be nonmonotonic. The properties calculated from the distribution of defect clusters exhibit stronger variations with density and dipole moment: both the mean size ( $\bar{N}_{cd}$ ) and the fraction of particles ( $\phi_{cd}$ ) in such clusters increase with increasing density and dipole moment.

A comparison of these properties, at a given thermodynamic state, for simulations with different numbers of particles reveals systematic differences that are more pro-

nounced at  $\mu^* = 2.75$ : the longer simulations of smaller systems, when compared to the shorter simulations of larger ones, exhibit larger rings corresponding to a much larger fraction of particles and a smaller fraction of particles in chains and defect clusters that exhibit relatively slow size variations. This is due to the fact that the small difference in the internal energy of the long and short runs, referred to above, has a dramatic effect on some of the structural properties. The lower internal energy of the longer runs is responsible for the self-assembly of larger rings and fewer chains and defect clusters. Note that the density dependence of the structural properties is unaffected by this systematic error at  $\mu^* = 2.5$  and  $2.75$ , but this may be the cause of the non-monotonic behavior of  $\bar{N}_c$  and  $\bar{N}_r$  with density, at  $\mu^* = 3.0$ .

### B. Length distributions

In Figs. 2, 3, and 4 we plot the equilibrium length distributions of chains, rings, and defect clusters obtained from simulations with  $N = 5776$  at  $\rho^* = 0.025, \mu^* = 2.5$  (a) and  $\rho^* = 0.0375, \mu^* = 3.0$  (b). Also plotted are simple histograms of these quantities. The distributions obtained for the other thermodynamic states are similar. From the figures we identify the difficulty in obtaining good statistics at large densities and/or dipole moments as the distributions broaden considerably. It is clear, however, that by smearing out the statistical noise by using simple histograms one obtains similar distributions with well defined peaks and decays for all the thermodynamic states. This suggests a scaling behavior that will be described in Sec. IV.

### C. Internal energy of chains and rings

We computed the internal energy per particle of chains and rings as a function of their size  $\epsilon_c(N)$  and  $\epsilon_r(N)$ , respec-

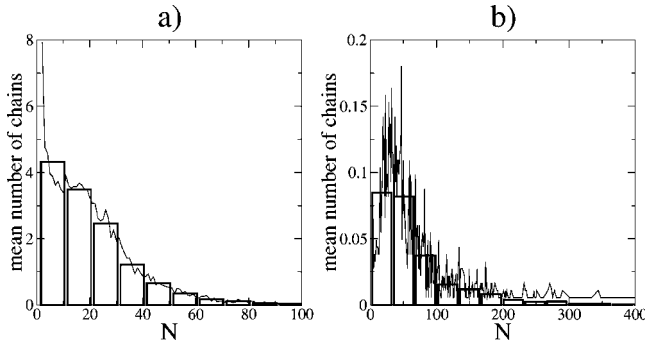


FIG. 2. Average number of chains of size  $N$  obtained from simulations at (a)  $\rho^*=0.025$ ,  $\mu^*=2.5$  (system with 5776 particles) and (b)  $\rho^*=0.0375$ ,  $\mu^*=3.0$ . The bars represent histograms obtained by simple averages in steps of size  $\bar{N}_c/2$ .

tively. For all the states considered  $\epsilon_r(N)$  is lower than  $\epsilon_c(N)$  if  $N \geq 4$  and the difference  $\epsilon_r(N) - \epsilon_c(N)$  exhibits a minimum for  $N \approx 8-10$ . In line with zero temperature results [24,25],  $\epsilon_c(N)$  and  $\epsilon_r(N)$  are well approximated (except for the smallest values of  $N$ ) by the functions

$$\frac{\beta \epsilon_c(N)}{\mu^{*2}} = -\epsilon_0^c + \frac{\epsilon_1^c}{N}, \quad (6)$$

and

$$\frac{\beta \epsilon_r(N)}{\mu^{*2}} = -\epsilon_0^r + \frac{\epsilon_1^r}{N^2}, \quad (7)$$

where the coefficients  $\epsilon_0^c$ ,  $\epsilon_0^r$ ,  $\epsilon_1^c$ , and  $\epsilon_1^r$  depend on  $\mu^*$  only and  $\beta \equiv 1/k_B T$ . We obtained these coefficients by fitting the simulation data to Eqs. (6) and (7). We found that for a given simulation the values of  $\epsilon_0^c$  and  $\epsilon_0^r$  differ by less than 1% and that their dependence on density is negligible. Thus, at a given temperature, the system has a well defined bond energy  $\epsilon_0(\mu^*) = \epsilon_0^c(\mu^*) = \epsilon_0^r(\mu^*)$ . In addition, we verified that  $\epsilon_1^c$  and  $\epsilon_1^r$  depend on temperature only. The values of these parameters are collected in Table II. Note that  $\epsilon_0$  is close to the nearest-neighbor dipolar approximation while  $\epsilon_1^c$

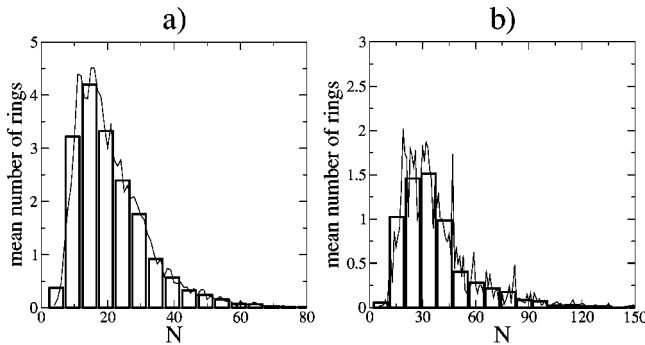


FIG. 3. Average number of rings of size  $N$  obtained from simulations at (a)  $\rho^*=0.025$ ,  $\mu^*=2.5$  (system with 5776 particles) and (b)  $\rho^*=0.0375$ ,  $\mu^*=3.0$ . The bars represent histograms obtained by simple averages in steps of size  $\bar{N}_r/4$ .

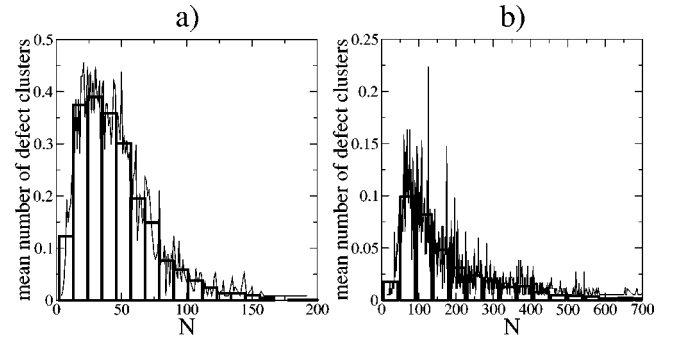


FIG. 4. Average number of defect clusters of size  $N$  obtained from simulations at (a)  $\rho^*=0.025$ ,  $\mu^*=2.5$  (system with 5776 particles) and (b)  $\rho^*=0.0375$ ,  $\mu^*=3.0$ . The bars represent histograms obtained by simple averages in steps of size  $\bar{N}_{cd}/4$ .

differs by about 25% [14]. In Fig. 5, we plot  $\epsilon_c(N)$  and  $\epsilon_r(N)$  obtained from the simulations at  $\rho^*=0.025, \mu^*=2.5$  ( $N=5776$ ) and  $\rho^*=0.0375, \mu^*=3$ , and the functions (6) and (7) calculated using the parameters of Table II. Similar results are obtained for the other simulations and thus we conclude that the internal energy of chains and rings is well approximated by the sum of a bond energy and a finite-size correction.

Also shown in Fig. 5 is the reduced energy per particle of defect clusters. The function for the internal energy of defect clusters is not known. However, a comparison of their energy with the energy of chains and rings reveals that the energy per particle is the same for all clusters, in the limit  $N \rightarrow \infty$ . The internal energy of defect clusters is always larger than that of rings and it appears to be larger than that of chains for small  $N$  only. This behavior, however, is within the statistical fluctuations of the energy and longer simulations are required to establish it.

#### D. Conformational properties of clusters

For large  $N$ , the radius of gyration  $R_g$  of the clusters scales with the number of monomers  $N$  as

$$R_g(N) = bN^\nu, \quad (8)$$

where  $b$  is a characteristic length and  $\nu$  a universal exponent that depends on the dimension of space and on the type of interactions and lies between 1 (rigid object) and 0.5 (random walk). Clusters with the conformation of a self-avoiding random walk (SARW) in 2D have  $\nu=0.75$  [26]. During the simulation runs, we calculated  $\langle R_g^2(N) \rangle$ , the mean value of the radius of gyration squared for chains, rings, and defect

TABLE II. Parameters of the internal energy of rings and chains.

$\mu^*$	$\epsilon_0$	$\epsilon_1^c$	$\epsilon_1^r$
2.5	2.05	2.56	$10 \pm 1$
2.75	2.12	2.65	$11 \pm 1$
3.0	2.17	2.66	$12 \pm 1$

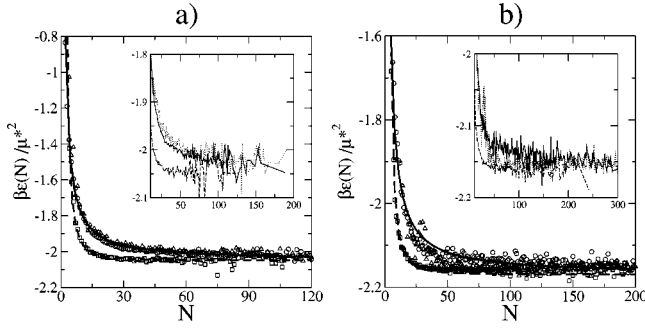


FIG. 5. Energy per particle (divided by  $\mu^{*2}$ ) of chains (circles), rings (squares), and defect clusters (triangles) of length  $N$  from simulations at (a)  $\rho^* = 0.025$ ,  $\mu^* = 2.5$  (system with 5776 particles) and (b)  $\rho^* = 0.0375$ ,  $\mu^* = 3$ . In the main figures lines are fits to the simulation data obtained using Eqs. (6) and (7) and the values of Table II. The inset shows the tails in more detail: full line corresponds to chains, dashed line to rings, and dotted line to defect clusters.

clusters of length  $N$ . In Figs. 6, 7, and 8 we plot the results for simulations at  $\rho^* = 0.025, \mu^* = 2.5$  and  $\rho^* = 0.0375, \mu^* = 3.0$ .

It is clear from Fig. 6 that  $\nu = 0.75$  for long chains ( $N$  greater than  $\approx 10$ ) and thus dipolar chains have the conformation of a 2D SARW. Similar results were obtained for all the other simulations and we conclude that the exponent is universal, in the range of densities and dipole moments considered in this work.

The radius of gyration of rings was calculated in a similar fashion and the results are shown in Fig. 7. It is clear from the figure that the scaling regime of SARWs with return to the origin (characterized by the same exponent  $\nu = 0.75$ ) is observed for large rings ( $N$  greater than  $\approx 40$ ). Smaller rings scale with  $\nu$  close to 1, indicating that they behave as rigid objects. The crossover from the rigid to the fluctuating (SARW) regime is broader at higher temperatures and lower densities.

A measure of the different stiffnesses of dipolar chains and rings is obtained through the persistence length of these clusters,  $\ell_c(N)$  and  $\ell_r(N)$ , respectively. The persistence

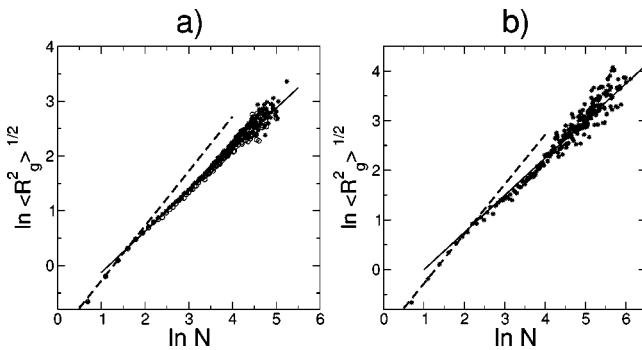


FIG. 6. Square root of the mean squared radius of gyration as a function of the number of monomers in chains: stars,  $N = 5776$ ; circles,  $N = 1600$ ; the full line has slope 0.75 and the dashed line slope 1. The radius of gyration is in units of  $\sigma$ . (a)  $\rho^* = 0.025$ ,  $\mu^* = 2.5$ ; (b)  $\rho^* = 0.0375$ ,  $\mu^* = 3.0$ .

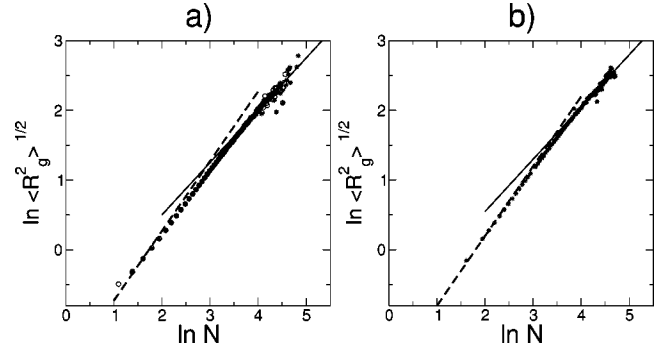


FIG. 7. Square root of the mean squared radius of gyration as a function of the number of monomers in rings: stars,  $N = 5776$ ; circles,  $N = 1600$ ; the full line has slope 0.75 and the dashed line slope 1. (a)  $\rho^* = 0.025$ ,  $\mu^* = 2.5$ ; (b)  $\rho^* = 0.0375$ ,  $\mu^* = 3.0$ .

length of chains may be calculated in a simulation run using [1]

$$\frac{\ell_c(N)}{\sigma} = \frac{1}{2\sigma^2} \left\langle \sum_{i=2}^{N-1} \vec{e}_1 \cdot \vec{e}_i + \vec{e}_{N-1} \cdot \vec{e}_{N-i} \right\rangle, \quad (9)$$

where  $\langle \dots \rangle$  is an average over chains of length  $N$ ,  $\vec{e}_i$  is the vector between consecutive dipoles ( $\vec{e}_i = \vec{r}_{i+1} - \vec{r}_i$ ) and 1, and  $N$  label the (free) chain ends. Clearly, Eq. (9) yields  $\ell_c(N) \approx N$  for rigid chains while  $\ell_c(N) \ll N$  for long flexible chains.

A similar expression, measuring the deviation from the rigid ring structure, may be used to calculate the persistence length of rings. The positions of the dipoles in the ring are labeled consecutively and the vectors  $\vec{e}_i$  between consecutive dipoles are defined as for chains but with periodic boundary conditions ( $\vec{e}_{i+N} = \vec{e}_i$ ). The ring persistence length  $\ell_r(N)$  is then obtained using

$$\frac{\ell_r(N)}{\sigma} = \frac{1}{N\sigma^2} \left\langle \sum_{i=1}^N \sum_{j=i+1}^{N-1+i} \vec{e}_i \cdot \mathbf{A}(\alpha_{ij}) \vec{e}_j \right\rangle, \quad (10)$$

where  $\mathbf{A}$  is the rotation matrix in 2D and  $\alpha_{ij} = 2\pi(i-j)/N$  is the angle between  $\vec{e}_i$  and  $\vec{e}_j$  in the ring configuration. For rigid rings Eq. (10) yields  $\ell_r(N) \approx N$  while for long flexible rings  $\ell_r(N) \ll N$ .

The persistence length of dipolar chains and rings is plotted in Fig. 8. Histograms, with the step size indicated in the caption, are calculated to smear out the statistical noise for large  $N$ . The results indicate that  $\ell_c(N)$  is constant within the statistical error while  $\ell_r(N)$  displays two regimes: it increases linearly with  $N$  at small  $N$  reaching a constant value at large  $N$ . The crossover between the rigid and SARW regimes occurs at larger values of  $N$  at lower temperatures. This clarifies the origin of the crossover for the radius of gyration of rings observed in Figs. 7(a) and 7(b).

Finally, we calculated the radius of gyration of defect clusters to check if they follow the conformational scaling of a RW ( $\nu = 0.5$ ) as they are rather convoluted objects. The results are plotted in Fig. 9. Care must be taken in analyzing these results since defect clusters have a variety of topologies

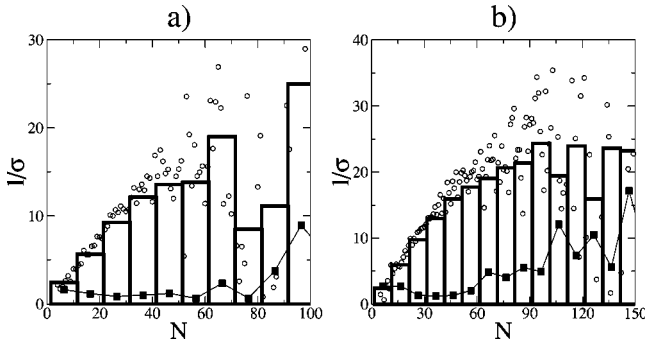


FIG. 8. Persistence length of chains and rings as a function of the number of monomers. Rings: open circles and bars (histogram). Chains: squares (histogram). The step size of both histograms is 10. (a)  $\rho^* = 0.025$ ,  $\mu^* = 2.5$ ; (b)  $\rho^* = 0.0375$ ,  $\mu^* = 3.0$ .

that were not distinguished in this calculation. In addition, their length distribution functions are broader than the distributions of chains and rings and thus larger statistical errors are to be expected. Nevertheless, the results of Fig. 9 show no evidence of a RW regime. We conclude that, for the finite systems studied in this work, defect clusters have the conformational properties of a SARW.

#### IV. SCALING LAWS FOR THE LENGTH DISTRIBUTIONS OF CHAINS AND RINGS: EQUILIBRIUM POLYMER THEORY

##### A. General results

The results of the previous section show that the structure of the dipolar fluid at low temperatures and densities may be described by equilibrium distributions of clusters of various types. Each type of cluster exhibits a well defined length distribution although clusters break and recombine during a simulation run. Their internal energy is consistent with a characteristic bond energy identical for all types of clusters. Finally, the total bond energy is very close to the total internal energy indicating that interactions between clusters are negligible.

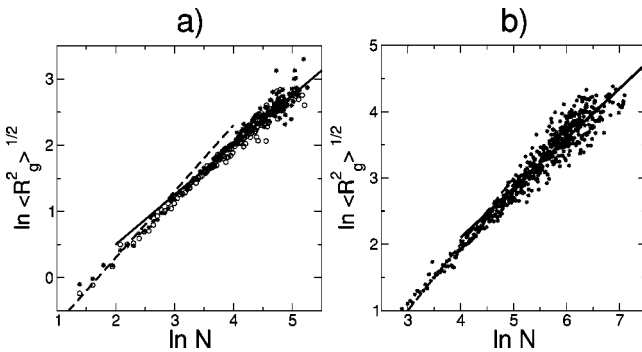


FIG. 9. Square root of the mean squared radius of gyration as a function of the number of monomers in defect clusters: stars,  $N = 5776$ ; circles,  $N = 1600$ ; the full line has slope 0.75 and the dashed line slope 1. (a)  $\rho^* = 0.025$ ,  $\mu^* = 2.5$ ; (b)  $\rho^* = 0.0375$ ,  $\mu^* = 3.0$ .

These features suggest that the quasi-2D dipolar fluid may be described as an ideal mixture of various types of clusters in chemical equilibrium [9]. The Helmholtz free energy density  $F/A$  of this system is written as

$$\beta\sigma^2 F/A = \sum_k \sum_{N=s_k}^{\infty} \rho_k^*(N) \times [\ln \rho_k^*(N) - 1 - \ln \tilde{q}_k(N)], \quad (11)$$

where  $k$  labels the type of cluster (chains, rings, and the several types of defect clusters),  $s_k$  is the minimal length of clusters of type  $k$ , while  $\tilde{q}_k(N)$  is the partition function (multiplied by  $\sigma^2/A$ ) and  $\rho_k^*(N)$  the reduced density of clusters of type  $k$ , with length  $N$ .

Minimization of the free energy with respect to the densities  $\rho_k^*(N)$  yields the set of equations

$$\rho_k^*(N) = \tilde{q}_k(N) \exp(N\beta\mu), \quad (12)$$

where  $\mu$  is the chemical potential of the system. The cluster densities satisfy the condition

$$\rho^* = \sum_k \sum_{s_k}^{\infty} N \rho_k^*(N), \quad (13)$$

and may be viewed as length distributions for the various types of clusters. These equations determine the structure and thermodynamics of the system, given the cluster partition functions  $\tilde{q}_k(N)$ : at fixed temperature and density, Eqs. (12) and (13) define the distribution functions  $\rho_k^*(N)$  and thus the structure of the system; substitution of these distributions into Eq. (11) yields the equilibrium free energy as a function of  $\rho^*$  and  $\mu^*$ . The theory can be applied to dilute dipolar fluids if the partition functions of dipolar chains, rings, and defect clusters are known.

The results for the conformational properties of dipolar chains and rings suggest that these aggregates behave as dilute polymers. In addition, the existence of chemical equilibrium among clusters suggests an analogy with equilibrium polymers [20,21]. In recent MC simulations, a 3D (lattice and off-lattice) model was proposed that, by construction, allows the self-assembly of linear clusters (chains and rings). The cluster internal energy is proportional to the number of bonds and there is no attraction between clusters (nearest-neighbor bonding interactions). The model was specifically built to study the equilibrium properties of polydisperse linear aggregates and very accurate results for their conformational properties, length distributions, etc., were obtained. It was found that the conformational properties of these model equilibrium polymers are identical to those of monodisperse quenched polymers. Additionally, the length distribution functions of the simulated equilibrium polymers scale as predicted theoretically [26] and the presence of rings does not affect the distribution of chains.

In the following we analyze the 2D dipolar fluid by adopting the hypothesis that dipolar chains and rings behave as dilute equilibrium polymers. This will be tested by compar-

ing the theoretical and simulated results for the dipolar chain and ring length distribution functions. Before we proceed, we note an important difference between the dipolar fluid and the model equilibrium polymers described in the previous paragraph. In the latter there are two bonding sites per monomer and thus the internal energy of the clusters is always proportional to the number of bonds. By contrast, cross-linked dipolar chains and rings have internal energies that differ from those of chains and rings and thus we call them defect clusters.

### B. Length distributions of dipolar chains

For nearest-neighbor bonding interactions the chain energy is independent of the chain conformation and thus the partition function of an isolated, long,  $N$ -monomer chain is approximated by the product of two terms: (i) the number of conformations of a SARW with  $N$  steps, in the limit  $N \rightarrow \infty$  [26] and (ii) the Boltzmann factor of the energy  $E_c(N)$  [20,21],

$$Z_c(N) = A_c N^{\gamma-1} \exp[-\beta E_c(N)]. \quad (14)$$

$\gamma$  is a universal exponent that depends on the dimension of space and on the type of interactions and  $A_c$  is a nonuniversal constant. Assuming that the partition function of a dipolar chain with  $N$ -monomers of diameter  $\sigma$ , in area  $A$ , is separable and that the reduced energy per monomer is given by Eq. (6), we obtain

$$Z_c^{\text{dip}} = \frac{A}{\sigma^2} A_c N^{\gamma-1} \exp(N \epsilon_0 \mu^{*2} - \epsilon_1^c \mu^{*2}). \quad (15)$$

Substituting this result into Eq. (12) we find for the reduced density of noninteracting,  $N$ -dipolar chains,

$$\rho_c^*(N) = A_c N^{\gamma-1} \exp(-\epsilon_1^c \mu^{*2} - \tilde{\mu} N), \quad (16)$$

where  $\tilde{\mu} = -\beta\mu - \epsilon_0 \mu^{*2}$  is the shifted chemical potential.

Comparison of the chain densities obtained from the simulations with those calculated using Eq. (16) requires an approximation for the (shifted) chemical potential  $\tilde{\mu}$ . This is achieved by approximating the chain density (16) by a continuous function, namely, a non-normalized gamma distribution. The first moment of this distribution yields,

$$\bar{N}_c \equiv \frac{\sum_{N=2}^{\infty} N \rho_c^*(N)}{\sum_{N=2}^{\infty} \rho_c^*(N)} \approx \frac{\int_0^{\infty} N \rho_c^*(N) dN}{\int_0^{\infty} \rho_c^*(N) dN} = \frac{\gamma}{\tilde{\mu}}, \quad (17)$$

i.e.,  $\tilde{\mu}$  is inversely proportional to the mean chain length  $\bar{N}_c$ .

The decay of the chain length distribution (see Fig. 2) is dominated by the exponential term, which depends on  $N$  through the scaled variable  $N/\bar{N}_c$ . This scaling form was used to plot the chain length distributions obtained from six different simulations. The results are shown in Fig. 10 where the theoretical prediction  $\ln[\rho_c^*(N)/\rho_c^*(\bar{N}_c)] \approx \gamma - \gamma N/\bar{N}_c$  with

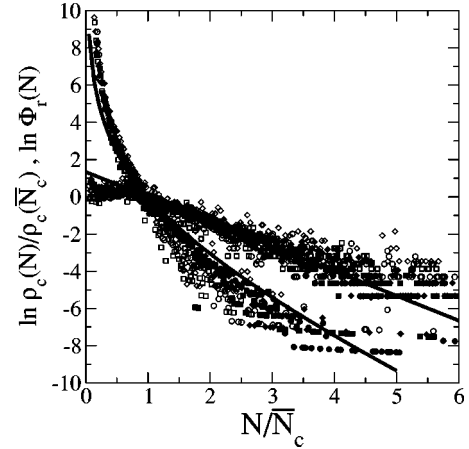


FIG. 10. Scaling form for the length distribution of dipolar chains and dipolar rings. Symbols are simulation results. Circles:  $\rho^* = 0.025$ . Squares:  $\rho^* = 0.03125$ . Diamonds:  $\rho^* = 0.0375$ . Full symbols:  $\mu^* = 2.5$ . Open symbols:  $\mu^* = 2.75$ . The results for chains straddle the straight line. The results for rings follow the curve and are obtained using Eq. (22). Full lines are the theoretical predictions: the straight line is the result for chains obtained from Eqs. (16) and (17) with  $\gamma = 1.33$  and the curve the result for rings obtained from the right-hand side of Eq. (23) with  $\gamma = 1.33$  and  $\alpha = 0.5$ .

$\gamma = 1.33$  [26] is also shown. The results suggest that scaling applies to systems at  $\mu^* = 2.5$ . For systems at  $\mu^* = 2.75$ , scaling obtains at small values of  $N/\bar{N}_c$  only, owing to the large statistical errors which increase with increasing  $\bar{N}_c$  and the decreasing fraction of monomers in chains. It is also clear from Fig. 10 that the scaling form does not apply to short chains ( $N < \bar{N}_c$ ). This is as expected since both Eq. (15) for the partition function and Eq. (6) for the chain internal energy are valid for large  $N$  only.

In Fig. 11 we plot the scaling form in a slightly different fashion that includes the logarithmic corrections arising from the power law in Eq. (16). We consider the normalized dis-

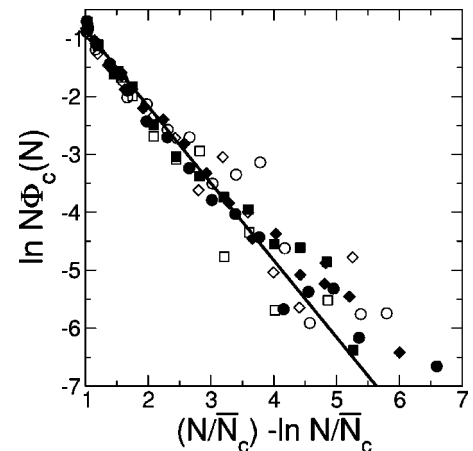


FIG. 11. Scaling form for the length distribution of chains using histograms and including logarithmic corrections [Eq. (18)]. Symbols are as in Fig. 10 and the full line is the theoretical prediction with  $\gamma = 1.33$ .

tribution of chains  $\Phi_c(N)$  corresponding to Eq. (16), and find,

$$\ln[N\Phi_c(N)] = K(\gamma) + \gamma \left( \ln \frac{N}{\bar{N}_c} - \frac{N}{\bar{N}_c} \right), \quad (18)$$

where  $K(\gamma) = \gamma \ln \gamma - \ln \Gamma(\gamma)$ . The left-hand side is obtained from the average fraction of chains with length in a given interval centered at  $N$  in the simulation run while the right-hand side is calculated using the theoretical value of  $\gamma = 1.33$ . The normalized distribution function is obtained from a histogram with step size  $\bar{N}_c/2$  (see Fig. 2), i.e.,  $\Phi_c(x)$  at  $x = (2k+1)\bar{N}_c/4$ , with integer  $k$ , is the average fraction of chains with length in the interval  $[x - \bar{N}_c/4; x + \bar{N}_c/4]$ . Figure 11 shows that the scaling form applies to intermediate values of  $N/\bar{N}_c$ . The scaling region is wider at low dipole moments and densities, in line with the fact that deviations from scaling for large  $N$  are due to statistical noise. As mentioned in the previous section, the number of chains in the simulations at  $\mu^* = 3$  is rather small, rendering the present analysis meaningless for that thermodynamic state.

We note that, in addition to smearing out statistical errors, histograms have the advantage over the bare distributions of being unaffected by changes in the cutoff distance  $r_c$ . We have repeated the histogram analysis for a system at  $\rho^* = 0.025, \mu^* = 2.5$ , and two different cutoff distances  $r_c$ ,  $1.1\sigma$  and  $1.2\sigma$ . As expected, the scaled distributions are not affected by the choice of cutoff.

### C. Length distributions of dipolar rings

As for chains the partition function of isolated, long,  $N$ -monomer rings may be approximated by the product of (i) the number of conformations of a SARW of  $N$  steps with return to the origin, in the limit  $N \rightarrow \infty$  [26] and (ii) the Boltzmann factor of the energy  $E_r(N)$  [20]. In addition, as remarked in [20], equilibrium between chains and rings has to be taken into account by including the possibility that  $N$ -rings may break in  $N$  different places, yielding an  $N$ -chain. The partition function of an  $N$ -ring is then

$$Z_r(N) = A_r N^{\alpha-3} \exp[-\beta E_r(N)]. \quad (19)$$

$\alpha$  is a universal exponent that depends on the dimension of space and on the type of interactions and  $A_r$  is a nonuniversal constant.  $\alpha$  obeys the hyperscaling relation  $\alpha = 2 - \nu D$ , and thus  $\alpha = 0.5$  for a SARW in  $D = 2$ . In analogy with the treatment of dipolar chains we assume that the partition function of dipolar rings is separable and use Eq. (19) to approximate the partition function of an  $N$ -dipolar ring, with internal energy given by Eq. (7), by

$$Z_r^{\text{dip}}(N) = \frac{A}{\sigma^2} A_r N^{\alpha-3} \exp \left( N \epsilon_0 \mu^{*2} - \frac{\epsilon_1^r}{N} \mu^{*2} \right). \quad (20)$$

Substitution of this equation into Eq. (12) yields for the densities of noninteracting  $N$ -dipolar rings

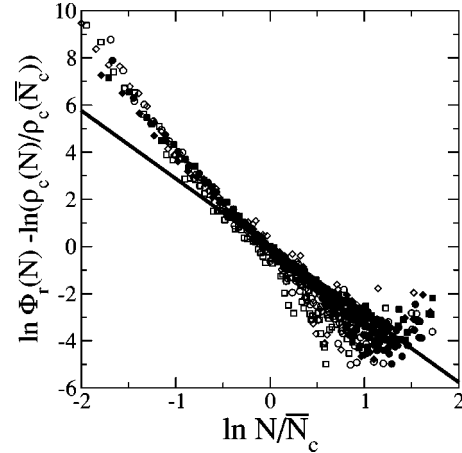


FIG. 12. Scaling form for the length distribution of dipolar rings using Eq. (24). Symbols are as in Fig. 10 and the full line is the theoretical prediction with  $\gamma = 1.33$  and  $\alpha = 0.5$ .

$$\rho_r^*(N) = A_r N^{\alpha-3} \exp \left( -\frac{\epsilon_1^r \mu^{*2}}{N} - \tilde{\mu} N \right). \quad (21)$$

Comparison of the simulation and theoretical results is carried out using the (auxiliary) distribution  $\Phi_r(N)$ ,

$$\Phi_r(N) = \frac{\rho_r^*(N)}{\rho_r^*(\bar{N}_c)} \exp \left[ \epsilon_1^r \mu^{*2} \left( \frac{1}{N} - \frac{1}{\bar{N}_c} \right) \right]. \quad (22)$$

By combining this equation with Eqs. (21) and (17) one finds that  $\Phi_r(N)$  is a universal function of  $N/\bar{N}_c$ , namely,

$$\ln \Phi_r(N) = \gamma + (\alpha - 3) \ln \frac{N}{\bar{N}_c} - \gamma \frac{N}{\bar{N}_c}. \quad (23)$$

We have calculated  $\Phi_r(N)$  using the average number of rings of a given length and the average number of rings with  $N = \bar{N}_c$  obtained in a simulation run as well as the value of  $\epsilon_1^r$  (see Table II). In Fig. 10 we plot  $\Phi_r(N)$  from six different simulations [Eq. (22)] and the right hand side of Eq. (23) calculated with  $\alpha = 0.5$  and  $\gamma = 1.33$ . The data collapse is remarkable. We may use the equilibrium chain length distribution to eliminate the exponential dependence of the ring distribution function, obtaining a slowly varying scaling function,

$$\ln \left( \frac{\Phi_r(N) \rho_c^*(\bar{N}_c)}{\rho_c^*(N)} \right) = (\alpha - \gamma - 2) \ln \frac{N}{\bar{N}_c}, \quad (24)$$

which is plotted in Fig. 12. The points in this figure are obtained by dividing the results corresponding to rings by those corresponding to chains in Fig. 10. The data collapse for the six simulation runs is again remarkable.

Figures 10 and 12 show that the simulation results scale according to the theoretical prediction, especially for intermediate values of  $N$ . In line with the results for the conformational properties scaling is not observed at small  $N$ . Statistical errors inherent in the simulations of the largest

clusters prevent scaling in the large  $N$  limit. Indeed, Fig. 10 and Fig. 12 show that the simulation results collapse on the theoretical curves for values of  $N$  between  $\approx \bar{N}_c$  and  $\approx 3\bar{N}_c$ . The slope of the straight line in Fig. 12 is consistent with  $\alpha=0.5$ , thus confirming the analogy between dipolar rings and equilibrium ring polymers. Again, departures from the straight line at small  $N$  can be traced to the crossover from rigid to flexible rings that occurs at relatively large values of  $N$ .

The generalization of this analysis to defect clusters is difficult for several reasons. The first concerns a limitation of the simulations: it is not feasible to obtain good statistics for all types of defect cluster (recall that the distributions of Fig. 4 lump together all types of defect cluster). Other difficulties arise in the calculation of the partition function of defect clusters, since the forms of both the internal energy and the configurational partition function are not well known.

## V. CONCLUSIONS AND DISCUSSION

Monte Carlo simulations of the quasi-2D dipolar fluid at low densities and temperatures reveal that the structure may be described in terms of equilibrium chains, rings, and defect clusters of more complex topology. The dipolar defect clusters have been characterized in detail.

The quantitative analysis of these structures shows that they exhibit length distribution functions that depend on the type of cluster and that vary with density and temperature. The calculation of the dipolar cluster internal energy reveals the existence of a bond energy that depends on temperature only. The analysis of the cluster conformational properties suggests that dipolar cluster conform as 2D standard polymers.

A detailed comparison of the length distributions of the simulated dipolar chains and rings with those predicted by equilibrium polymer theory shows that the structure of the quasi-2D dipolar fluid is the same as that of 2D equilibrium polymers.

As mentioned in the Introduction, the major question concerning dilute strongly dipolar fluids is the existence (and nature) of a fluid-fluid phase transition in this regime. The type of analysis developed in this paper, if extended to simulations at higher densities, may shed light on these questions. In fact, the mean chain length is a monotonically increasing function of the chemical potential [see Eq. (17) and the definition of  $\tilde{\mu}$ ] and depends on the total density  $\rho$  through  $\mu$  only. Likewise, the mean ring length [see Eq. (21)] is a

monotonic function of  $\mu$ . Thus, at fixed temperature, an instability signaled by  $(\partial\mu/\partial\rho)_T < 0$  may occur if  $\bar{N}_c$  and  $\bar{N}_r$  decrease in the same range of increasing densities. In other words, within simulation results as reported in this paper, the (mean field) loops that signal first-order phase transitions correspond to loops in the mean chain and ring lengths. This type of analysis has an advantage over the direct calculation of the free energy by making a connection between the structure and the thermodynamics of the system, thus revealing the mechanism that drives the phase transition. In fact, a necessary condition for the decrease of  $\bar{N}_c$  and  $\bar{N}_r$  with increasing density is the self-assembly of defect clusters. This conclusion is supported by the results of [20] for linear equilibrium polymers (chains and rings) where both these quantities are shown to increase with density at all simulated temperatures. Thus, the appearance of such loops indicates the existence of a topological phase transition [14] resulting from the competition between structures with high energy and high entropy (chains) and structures with low energy and low entropy (defect clusters). This method of determining the existence and nature of the phase transition has, however, severe limitations already evident in the results of Table I. In order to obtain reliable results for  $\bar{N}_c$  and  $\bar{N}_r$ , very long simulations are required. The number of chains, however, decreases rapidly with increasing density, and thus statistical errors may become unacceptable too soon. The mean ring length is less affected by statistical errors since the decrease in the number of rings with increasing density is rather slow.  $\bar{N}_r$ , however, varies more slowly with density, rendering the detection of nonmonotonic behavior more difficult. Despite these limitations we are currently simulating higher densities at reduced dipole moment  $\mu^*=2.75$  and will analyze the results along these lines.

In closing, we note that the topological phase transition is only one of the phase transitions that has been predicted to occur in dipolar fluids at low densities. According to recent theoretical proposals, these systems may also exhibit a percolation transition with increasing density [27]. The method developed in this paper could also be used to test this hypothesis. It is straightforward to establish the scaling form of the largest dipolar cluster and to compare it with the form of critical percolating clusters [28].

Other phase diagrams that include nematic-isotropic [29] or nematic-nematic [30] transitions have been proposed for models of semiflexible equilibrium polymers. It is, however, unlikely that ordered phases occur in dilute dipolar fluids.

- 
- [1] J.J. Weis and D. Levesque, Phys. Rev. Lett. **71**, 2729 (1993); D. Levesque and J.J. Weis, Phys. Rev. E **49**, 5131 (1994).
  - [2] M.J. Stevens and G.S. Grest, Phys. Rev. E **51**, 5962 (1995).
  - [3] M.E. van Leeuwen and B. Smit, Phys. Rev. Lett. **71**, 3991 (1993).
  - [4] J.M. Tavares, J.J. Weis, and M.M. Telo da Gama, Phys. Rev. E **59**, 4388 (1999).
  - [5] P.J. Camp and G.N. Patey, Phys. Rev. E **62**, 5403 (2000).
  - [6] R. van Roij, Phys. Rev. Lett. **76**, 3348 (1996).
  - [7] R.P. Sear, Phys. Rev. Lett. **76**, 2310 (1996).
  - [8] J.M. Tavares, M.M. Telo da Gama, and M.A. Osipov, Phys. Rev. E **56**, R6252 (1997).
  - [9] P.I.C. Teixeira, J.M. Tavares, and M.M. Telo da Gama, J. Phys.: Condens. Matter **12**, R411 (2000).
  - [10] J.-M. Caillol, J. Chem. Phys. **98**, 9835 (1993).
  - [11] Y. Levin, Phys. Rev. Lett. **83**, 1159 (1999).

- [12] Y. Levin, P.S. Kuhn, and M.C. Barbosa, *Physica A* **292**, 129 (2001).
- [13] P.J. Camp, J.C. Shelley, and G.N. Patey, *Phys. Rev. Lett.* **84**, 115 (2000).
- [14] T. Tlusty and S.A. Safran, *Science* **290**, 1328 (2000).
- [15] P. Pincus, *Science* **290**, 1307 (2000).
- [16] T. Tlusty, S.A. Safran, R. Menes, and R. Strey, *Phys. Rev. Lett.* **78**, 2616 (1997); T. Tlusty, S.A. Safran, and R. Strey, *ibid.* **84**, 1244 (2000).
- [17] Although defect particles are particles with any number of neighbors different from two, we have found it useful in the context of the simulations to distinguish end particles. In this work defect particles are those with more than two neighbors.
- [18] J.J. Weis, *Mol. Phys.* **93**, 361 (1998); W. Wen, F. Kun, K.F. Pál, D.W. Zheng, and K.N. Tu, *Phys. Rev. E* **59**, R4758 (1999); S.W. Davis, W. McCausland, H.C. McGahagan, C.T. Tanaka, and M. Widom, *ibid.* **59**, 2424 (1999); J.J. Weis, *Mol. Phys.* **100**, 579 (2002).
- [19] V.F. Puentes, K.M. Krishnan, and A.P. Alivisatos, *Science* **291**, 2115 (2001).
- [20] J.P. Wittmer, P. van der Schoot, A. Milchev, and J.L. Barrat, *J. Chem. Phys.* **113**, 6992 (2000).
- [21] J.P. Wittmer, A. Milchev, and M.E. Cates, *J. Chem. Phys.* **109**, 834 (1998).
- [22] G.T. Gao, X.C. Zeng, and W. Wang, *J. Chem. Phys.* **106**, 3311 (1997).
- [23] E. Lomba, F. Lado, and J.J. Weis, *Phys. Rev. E* **61**, 3838 (2000).
- [24] P. Jund, S.G. Kim, D. Tomanek, and J. Hetherington, *Phys. Rev. Lett.* **74**, 3049 (1995).
- [25] P.C. Jordan, *Mol. Phys.* **38**, 769 (1979).
- [26] J. des Cloizeaux and G. Jannink, *Les Polymères en Solution* (Les Éditions de Physique, Les Ulis, 1987).
- [27] R.P. Sear and J. Cuesta, *Europhys. Lett.* **55**, 451 (2001).
- [28] A. Coniglio, *J. Phys.: Condens. Matter* **13**, 9039 (2001).
- [29] A. Chatterji and R. Pandit, *Europhys. Lett.* **54**, 213 (2001).
- [30] J.T. Kindt and W.M. Gelbart, *J. Chem. Phys.*, **114**, 1432 (2001).